Shock-induced phase transformations in gallium single crystals by atomistic methods

Kai Kadau,[1,*] Frank J. Cherne,[2,†] Ramon Ravelo,[3,‡] and Timothy C. Germann[1,§]
[1]*Theoretical Division, Los Alamos National Laboratory, Los Alamos, New Mexico 87545, USA*
[2]*Weapons Experiments Division, Los Alamos National Laboratory, Los Alamos, New Mexico 87545, USA*
[3]*Physics Department, The University of Texas at El Paso, El Paso, Texas 79968, USA*
(Received 21 May 2013; revised manuscript received 18 September 2013; published 29 October 2013)

Utilizing a modified embedded atom method potential, we performed large-scale classical molecular dynamics simulations (with up to 50 million atoms) to investigate the response of Ga single crystals to shock compression along the three major orientations of the orthorhombic A11 ground state, i.e., [001], [010], and [100]. For weak shocks with particle velocity $u_p < 300$ m/s, these defect-free single crystals respond elastically, but for stronger shocks, they undergo a structural phase transformation and then (for even stronger shocks) melt. For intermediate shock strengths (300 m/s $< u_p <$ 1.2 km/s) a split shock wave is formed, with an elastic precursor (uniaxial compression wave) leading the slower transformation wave. The transformed region consists of a mixed phase, with stripes of the product phase embedded into the uniaxially compressed parent phase, with the ratio of product to parent phase increasing with increasing shock strength, much like in martensitic phase transformations. Upon shock release from the free surface at the end of the sample, the transformation is reversed, leaving only some defects behind, which makes it difficult to experimentally investigate the structural transformation in shock-recovered samples. We investigated the structure produced by the shock and found it to be similar to the β phase of Ga which is obtained by supercooling from the liquid state. However, the product phase shows only half the period along [100] in the calculated diffraction pattern. Further investigation showed that this is due to a different stacking sequence in this direction, namely ABCD instead of AB for the β phase.

DOI: 10.1103/PhysRevB.88.144108 PACS number(s): 71.15.Pd, 62.50.−p, 81.30.Kf, 62.20.−x

I. INTRODUCTION

The existence of Gallium (Ga) was first postulated by the Russian chemist Dimitri Mendeleev and independently discovered in 1885 by the French chemist Paul E. Lecoq de Boisbaudran, who named the soft silvery metallic solid *gallia*, from the Latin word *Gallia* after his homeland.[1] Ga is brittle at low temperatures and has a very low melting point of 302.9 K, i.e., it melts in one's hand. The most popular use of Ga is in the semiconductor industry in form of gallium arsenide and gallium nitride, which are used in many electronic components.

As a relatively small element (atomic number 31), Ga attacks steel and other metals by diffusing easily into grain boundaries, which makes them brittle. However, small amounts of Ga can be used to stabilize certain crystallographic metallic phases. For instance, up to 1 wt.% Ga is used to stabilize the most easily machineable face-centered-cubic (fcc) δ phase of Pu over a wide pressure and temperature range.[2]

The complexity of high-pressure and nonequilibrium phases in elemental metals such as Ga has been reviewed by McMahon and Nelmes.[3] In particular for Ga, new complex high-pressure phases have been revealed by x-ray angle-dispersive powder diffraction.[4] The latter makes Ga a very interesting prototype for studying complex nonequilibrium phase transformations, such as the shock-induced transformations, which can occur in polymorphic materials.[5]

The ground state of Ga is the orthorhombic A11 α-Ga phase [also known as Ga (I)], which has a complex dimerized structure as illustrated in Fig. 1. One can think of it as a distorted fcc lattice with Ga dimers of two alternating orientations occupying the fcc lattice sites. Due to this very open ground-state structure, the density actually *increases* upon melting; this implies that pressure-induced melting of Ga (I) is possible (see Fig. 2), as also occurs in solid ice. Besides equilibrium phases such as the aforementioned Ga (I), Ga (II), and Ga (III) (see Fig. 2), many metastable structures have been discovered. For instance, the metastable β-Ga phase is often formed by solidification of a supercooled liquid; its structure is also an open dimerized system, as shown in Fig. 3.

The crystallographic dependence of shock response in single crystals has been investigated by nonequilibrium molecular dynamics (NEMD) for fcc materials[6–10] and for iron, which undergoes a shock-induced phase transformation from the body-centered cubic (bcc) to the close-packed hexagonal-close-packed (hcp) and fcc structures.[11,12] Prompted by these latter simulation studies, *in situ* x-ray diffraction experiments subsequently confirmed the NEMD predictions for Fe single crystals compressed in the [100] crystallographic direction.[13–15] More recently, NEMD simulations have been used to investigate atomic-scale plastic deformation processes in more complex crystal structures beyond these relatively simple fcc, hcp, and bcc lattices. For instance, the mechanical (i.e., nonreactive) shock response of the high-explosive crystals HMX[16] and RDX[17] have been reported. However, aside from the widespread interest in iron,[18] shock-induced phase transformations between two stable crystal polymorphs with more open and complex (and therefore more difficult to analyze) structures have not been widely studied. In the present work, we report NEMD simulations of such a shock-induced polymorphic phase transformation in single-crystal Ga, resulting in a previously unreported "β-stacking fault" structure whose (meta-)stability is probed by density functional theory calculations.

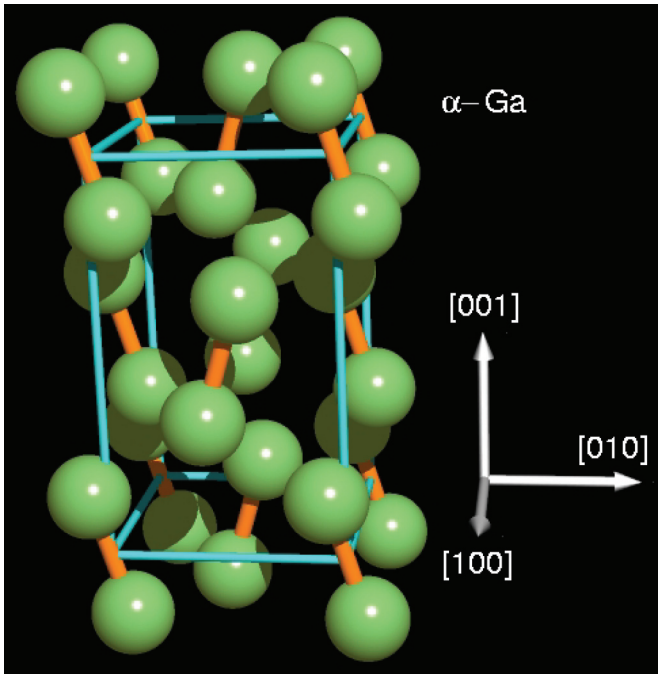

FIG. 1. (Color online) The orthorhombic A11 α-Ga ground-state structure or Ga (I).

II. METHODS

A. Modified embedded atom method (MEAM)

In order to describe high-pressure and nonequilibrium phenomena on an atomistic level, we utilize a modified embedded-atom method (MEAM) force field to describe the interaction between individual atoms.[19] MEAM incorporates three-body terms which are capable of describing complex

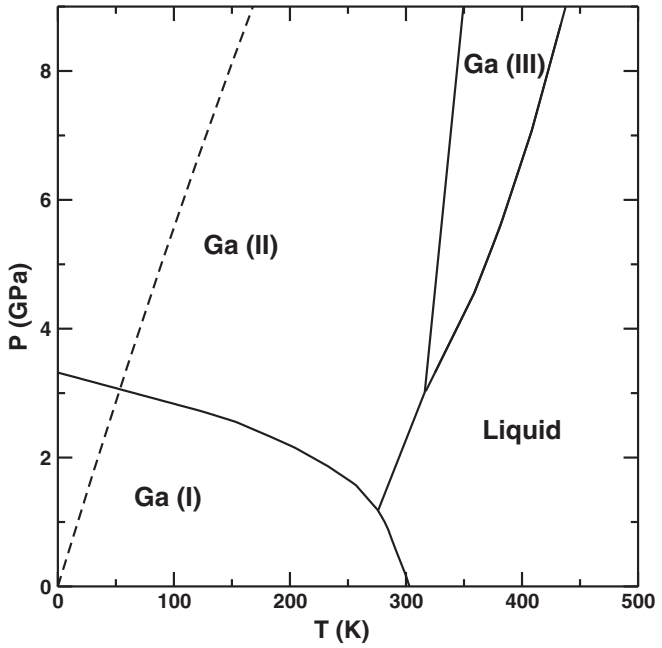

FIG. 2. The phase diagram of Ga. The dashed line indicates possible shocked states as extrapolated from simulation results in the overdriven regime (see Sec. III A).

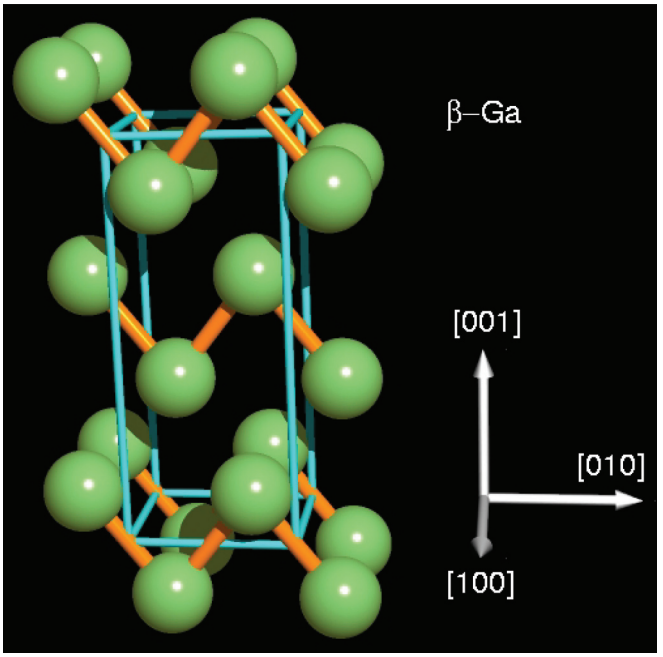

FIG. 3. (Color online) The metastable β-Ga structure is oftentimes found after the supercooled liquid solidifies.

open structures such as the Ga structures mentioned in Sec. I. Such empirical potentials describe in an effective manner how the energy landscape changes as a function of atomic arrangements. The parametrization and structure of the MEAM potential is motivated by electronic structure formalisms and their descriptions. For instance, MEAM applies the concept of a third atom screening the electronic density between a pair of atoms via an ellipse construction.[20]

In the MEAM methodology, we specify the total potential energy E of a system with N atoms and different atom species:

$$E = \sum_{i}^{N} F(\bar{\rho}_i) + \frac{1}{2} \sum_{i}^{N} \sum_{j \neq i}^{N} \phi(r_{ij}). \tag{1}$$

Here, F is the embedding function for the species of the atom i and ϕ is the pair potential between atom i and j at sites $\mathbf{r}_i$ and $\mathbf{r}_j$, respectively. The absolute distance between the atoms is denoted as r_{ij}. The electronic density at the site $\mathbf{r}_i$ is given by

$$\bar{\rho} = \rho^{(0)} G(\Gamma), \tag{2}$$

with

$$\rho^{(0)} = \sum_{j \neq i} \rho^{a(0)}(r_{ij}) \tag{3}$$

representing the s-orbital contribution to the electronic density.

The function

$$\Gamma = \sum_{h=1}^{3} t^{(h)} \left(\frac{\rho^{(h)}}{\rho(0)} \right)^2 \tag{4}$$

takes into account the angular dependence. Within this framework, the angle-dependent terms of the electron densities representing the p, d, and f-orbital contributions are written

as

$$(\rho^{(1)})^2 = \sum_{\alpha}\left[\sum_{j\neq i}\rho^{a(1)}(r_{ij})\frac{r_{ij}^{\alpha}}{r_{ij}}\right]^2,$$

$$(\rho^{(2)})^2 = \sum_{\alpha\beta}\left[\sum_{j\neq i}\rho^{a(2)}(r_{ij})\frac{r_{ij}^{\alpha}r_{ij}^{\beta}}{r_{ij}^2}\right]^2 - \frac{1}{3}\left[\sum_{j\neq i}\rho^{a(2)}(r_{ij})\right]^2,$$

$$(\rho^{(3)})^2 = \sum_{\alpha\beta\gamma}\left[\sum_{j\neq i}\rho^{a(3)}(r_{ij})\frac{r_{ij}^{\alpha}r_{ij}^{\beta}r_{ij}^{\gamma}}{r_{ij}^3}\right]^2 - \frac{3}{5}\sum_{\alpha}\left[\sum_{j\neq i}\rho^{a(3)}(r_{ij})\frac{r_{ij}^{\alpha}}{r_{ij}}\right]^2, \quad (5)$$

with α,β,γ superscripts denoting the Cartesian (x, y, z) components of the $\mathbf{r}_{ij} = \mathbf{r}_i - \mathbf{r}_j$ interatomic distance vector. The atomic densities $\rho^{a(h)}$ are usually represented by exponential functions, and similar physically motivated analytic functional forms are used for $F(\rho_i)$, $G(\Gamma)$, and $\phi(r_{ij})$.[19–21] The $G(\Gamma)$ term represents a scaling of the electronic density based on its angular dependence. In addition, a radial cutoff function is introduced which ensures that the atomic densities $\rho^{a(h)}(r_{ij})$ and pair potentials $\phi(r_{ij})$ go smoothly to zero for $r_{ij} \geqslant r_c$. This short-range nature of the MEAM interaction enables the implementation of an efficient linear-scaling algorithm which, together with the IBM/LLNL BlueGene/L supercomputer, was required to perform the multimillion-atom simulation studies presented here.

The effect of electronic density screening is taken into account by considering a pair of atoms i and j with a distance r_{ij} smaller than the radial cutoff distance r_c. As illustrated by Baskes,[20] we can define a screening ellipse with a minor axis to be the connection between atoms i and j, rotated to lie on the x axis of a two-dimensional Cartesian coordinate system (x,y). In this coordinate system, the atoms i and j are mirror symmetric to each other with respect to the y axis. The ellipse is then defined by

$$x^2 + \frac{1}{C}y^2 = \left(\frac{1}{2}r_{ij}\right)^2. \quad (6)$$

A third atom k, with distances r_{ik} and r_{jk} from atoms i and j, respectively, is considered to completely screen the interaction between atoms i and j, if atom k is within the ellipse with the parameter $C_{\min}$. When this occurs, the pair potential between the two atoms i and j, the atomic density at atom i given by atom j, and the atomic density at atom j given by atom i are all set to zero. If atom k is outside the ellipse with the parameter $C_{\max}$, it does not influence the pair. In between these two limiting ellipses, atom k partially screens the interaction between atoms i and j, whose pair potential and electronic densities are each multiplied by the screening factor

$$S_{ijk} = f_c\left[\frac{C - C_{\min}}{C_{\max} - C_{\min}}\right], \quad (7)$$

with

$$C = \frac{4r_{ik}^2r_{ij}^2 - \left(r_{ik}^2 - r_{jk}^2 + r_{ij}^2\right)^2}{r_{ij}^4 - \left(r_{ik}^2 - r_{jk}^2\right)^2}, \quad (8)$$

and

$$f_c(x) = \begin{cases} 1, & x \geqslant 1 \\ [1-(1-x)^4]^2, & 0 < x < 1 \\ 0, & x \leqslant 0 \end{cases}. \quad (9)$$

This procedure has to be done for all atoms k (except if one atom screens the pair completely) that are in the neighborhood of the pair ij such that the screening factor for this pair can be written as

$$S_{ij} = \prod_{k\neq i,j} S_{ijk}. \quad (10)$$

In order to calculate the screening for one pair of atoms, one has to pass over all possible neighbors of the pair that are within the outer screening ellipse (i.e., that with ellipse parameter $C_{\max}$).

Using this generic approach, MEAM parameters can be fit to reproduce important material properties for the system and conditions of interest. Here, we use MEAM parameters that were primarily fit to various properties of a hypothetical fcc phase based on *ab initio* calculations; included were the relative energies to other phases including the A11 Ga(I) ground-state phase of solid Ga.[21] For very high densities, or short distances, the interaction potential is often smoothly transitioned to the generic Biersack and Ziegler[22] repulsive pair potential, in order to provide physically realistic energies at the very short interaction distances which arise in energetic collision cascades. This transition typically begins at interatomic distances slightly beyond the short interatomic distance of Ga dimers within the A11 Ga(I) ground-state structure (see Fig. 1); however, in the present work we utilize the pure MEAM functional form without any short-range "ZBL" spline.

B. Nonequilibrium molecular dynamics (NEMD) simulation method

In order to understand a material's response to dynamic loading on an atomistic scale, the dynamics of the individual atoms comprising that material have to be calculated. This means solving a coupled system of second order differential equations for the movement of N atoms, whereby the forces are calculated by utilizing a force-field such as the MEAM potential described above.

For this, we employed the high-performance scalable parallel short-range molecular-dynamics code SPASM,[23–25] and initiated shock waves by a "momentum mirror" that is positioned at the "left" side of an elongated sample.[6] A defect-free single-crystal sample elongated in the specified crystallographic direction is created, and atoms are given random velocities assigned such that the initial temperature is 5 K. This low temperature is chosen in order to facilitate analysis of the structural transformation and to delay the onset of melting. In addition to these thermal velocities, all atoms are given an additional piston or particle velocity u_p directed towards the momentum mirror. This perfectly flat and infinitely massive mirror specularly reflects any atoms reaching it, resulting in

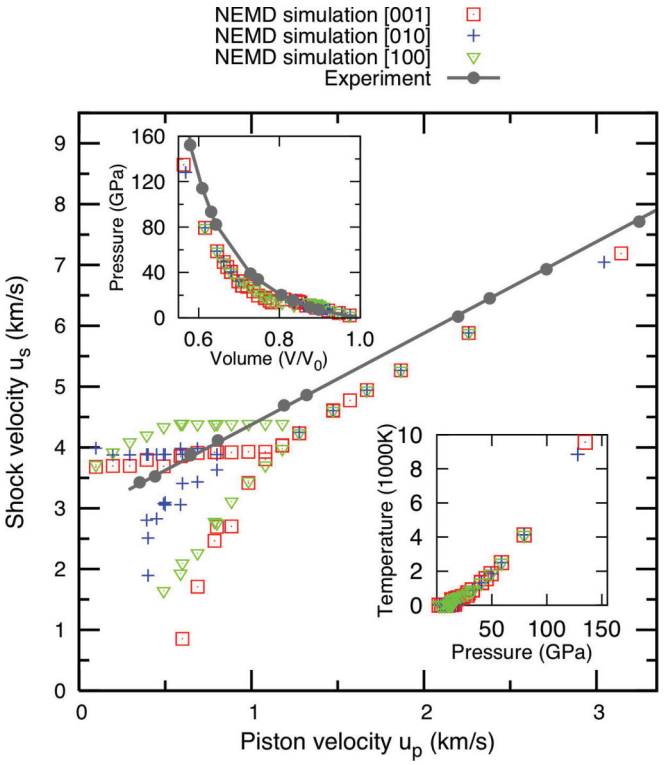

FIG. 4. (Color online) Shock hugoniot of single-crystal Ga for three different crystallographic shock directions and an initial temperature of approximately 5 K. The experiments of Fritz and Carter[28,29] started from ambient conditions in the liquid phase.

a shock wave in the material with velocity u_s traveling away from the mirror.[6,11] This methodology has been applied and successfully ported to the BlueGene/L architecture.[25,26] For instance, a sample containing about 50 million Ga atoms was simulated on 16 384 BlueGene/L cores for about 73 000 time steps (see Fig. 9). This results in 0.074 ns physical simulation time and took close to 20 h to simulate, including periodic calculation of correlation functions and an *in situ* rendering of multiple images[27] every 1000 integration steps. Smaller samples containing about 20 million atoms and less were also performed.

The resulting nonequilibrium response of Ga(I) to shock loading along [001], [010], and [100] (see Fig. 1 for definition of the crystallographic directions) is analyzed by calculating local average properties such as particle velocity, density, pressure, and temperature, as well as analyzing the atomic configurations in real and Fourier space, as discussed in the next section.

III. RESULTS

A. Shock hugoniot

The hugoniot, i.e., the locus of shocked states, was calculated for Ga by NEMD for shock loading along [001], [010], and [100] and compared to experimental results from Fritz and Carter,[28,29] which started from ambient conditions in the liquid state (see Fig. 4). For low shock strengths, the orientation dependence of the hugoniot is clearly visible in the u_p-u_s representation, as the anisotropy of the single crystal has a strong influence. Furthermore, in the u_p-u_s representation, a faster elastic precursor and a slower transformation wave can be seen. As the shock strength increases, the effect of anisotropy vanishes and only one branch of the hugoniot for all directions exists. Similar observations have been made for shock-induced phase transformations in Fe single crystals.[11,12] In the case of Fe, modeled by an embedded-atom method (EAM) potential[30,31] without the many-body angular term, the experimental hugoniot pressure is below the NEMD data.[11] The experimental liquid hugoniot data are slightly stiffer as a function of pressure than the NEMD data. Upon melting of solid Ga, a volume contraction takes place, making the liquid more dense than the solid and causing the melting point to decrease with increasing pressure (i.e., a negative Clapeyron slope). We have previously demonstrated that the present MEAM potential captures this anomalous melting behavior, and that with a slight modification, can exhibit improved agreement with the experimental liquid hugoniot.[29] There have been no experiments to look at the effect upon the u_p-u_s relations upon going through an anomalous melt transition.

B. [010] shock direction

For weak shock strengths, a split two-wave structure with a faster uniaxially compressed elastic front and a slower transformation wave is observed. In Fig. 5, snapshots for four different shock velocities for shocks in the [010] direction are presented. For the weakest shock ($u_p = 400$ m/s), the separation between the uniaxially compressed elastic precursor and the following mixed-phase region is largest, decreasing with increasing shock strength. At the same time, the amount of the needlelike product phase (visible as magenta-colored regions) increases, with the size of the needles decreasing with increasing shock strength. The two distinct waves are more clearly observed in particle velocity profiles (see Fig. 6). The slight increase before the elastic precursor in this particular shock direction has been associated with rotation of dimers around [100] (see Fig. 1) and is not observed for shocks along the other directions (see Figs. 7 and 8). For the strongest shock shown in this panel ($u_p = 800$ m/s), the shock is almost overdriven, i.e., the transformation wave is close to the elastic precursor wave, and exhibits an amorphous solid or molten liquid phase at the left side of the sample.

Once the shock wave reaches the free surface, the sample is able to unload via a rarefaction fan which spreads as it moves back towards the momentum mirror impact surface. From inspection of several simulations carried out long enough to reach this point (see Supplemental Material for movies of the process[32,33]), we find that the mixed-phase structure quickly reverts to the A11 parent structure upon release. Based on this observation, we note that experimental *post situ* analysis of shock-recovered samples may not have any signatures of the shock-induced structural phase transformation found in these simulations, since the transition is largely (if not entirely) reversible. However, as discussed below in Sec. III E, *in situ* x-ray diffraction diagnostics would be able to conclusively confirm (or disprove) the structural transformation indicated by our NEMD simulations.[13–15]

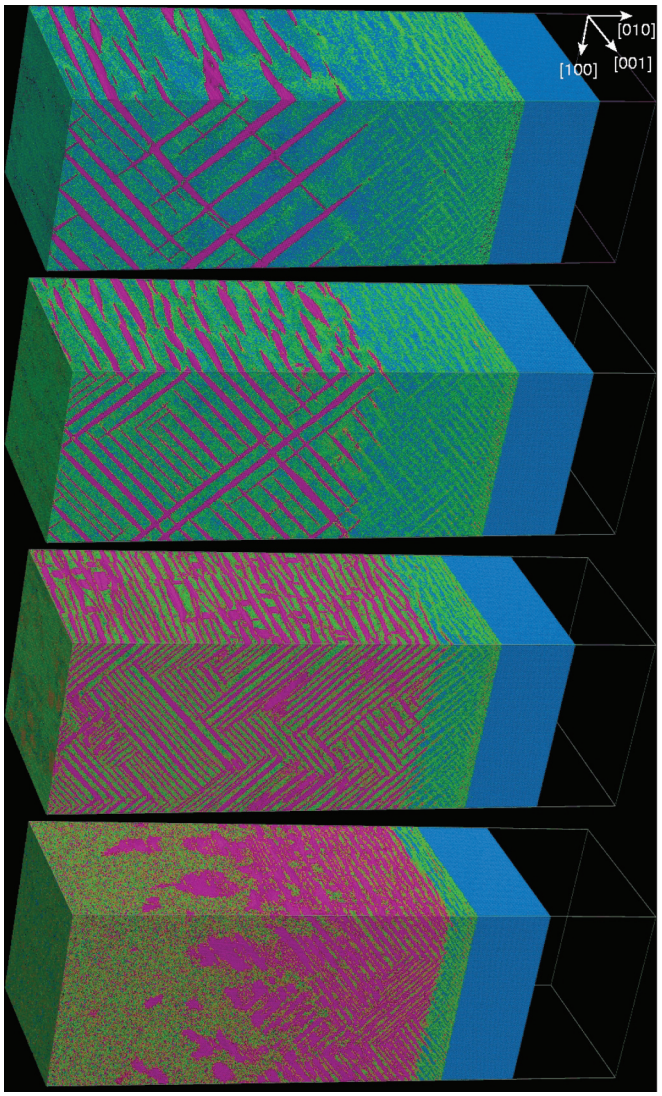

FIG. 5. (Color online) Ga single crystals shocked along the [010] direction shown 35.6 ps after impact with a momentum mirror on the left induced a shock wave traveling to the right. Four increasing shock strengths are shown: $u_p = 400$, 450, 600, and 800 m/s from top to bottom, respectively. Atoms are colored by the number of neighbors n within a distance of 0.255 nm (a dimer distance is 0.246 nm): 1 = blue, 2 = green-blue, 3 = green, 4 = orange, 5 = magenta, and 6 = red. An elastic precursor (blue/green) can be seen ahead of the product phase (magenta). The temperature, pressure, and shock velocity of the elastic (plastic) region from top to bottom are 11 K, 8.0 GPa, and 3.9 km/s (29 K, 8.6 GPa, and 1.9 km/s); 11 K, 8.1 GPa, and 3.9 km/s (38 K, 10.0 GPa, and 2.8 km/s); 12 K, 8.6 GPa, and 3.9 km/s (62 K, 13.8 GPa, and 3.4 km/s); 12 K, 9.3 GPa, and 3.9 km/s (70 K, 18.8 GPa, and 3.6 km/s), respectively. Each sample contains 20.6 million atoms in a 49.8 nm × 50.6 nm × 160.5 nm geometry.

C. [100] shock direction

For shock compression along the [100] direction, elastic precursor waves followed by a slower transformation wave are also exhibited (see Fig. 7). In front of the shock wave and ahead of the elastic precursor, oscillations in the particle velocity profile are visible. The oscillations can also be seen in the neighbor count colored figures showing the positions

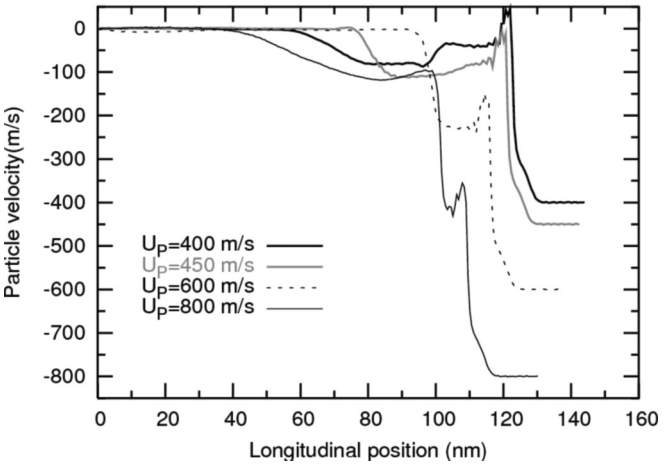

FIG. 6. Particle velocity profiles corresponding to the [010]-loaded samples shown in Fig. 5.

of the atoms (top of Fig. 7). These oscillations have earlier been observed for shock waves along "stiff" directions and associated with solitons.[7,12] For this direction, the same product structure as for [010] compression (magenta stripes) is also observed. For $u_p = 800$ m/s, the material quickly transforms into a melted/amorphous state, which is also observed for $u_p = 600$ m/s near the shock-inducing piston face.

D. [001] shock direction

Shock waves initiated along the [001] direction have a larger neighbor count in their elastic precursor regime which can be understood by looking at Fig. 1. By compressing the lattice in [001] direction—which is basically the dimer direction—the dimers of different lattice sites come close to each other. The elastic precursor along this direction is visible as red atoms with green regions in Fig. 8. The magenta product phase is also observed. For $u_p = 800$ m/s, the material quickly transforms into a melted or amorphous arrangement, which can also be seen for $u_p = 600$ m/s near the piston face. Although not as pronounced as in the case of shocks along [100], oscillations of the particle-velocity profiles slightly ahead of the precursor and in the precursor are observed.

E. Analysis of shock-induced structural changes

Having observed a solid-solid phase transformation in all three directions, we next analyze the structure of this product phase (shown in magenta in Figs. 5, 7, and 8. In order to have a sufficiently large volume to analyze, a simulation containing over 50 million atoms was performed for a particle velocity of $u_p = 500$ m/s and loading in the [010] direction. Movies illustrating the entire loading and unloading process are available as Supplemental Material, and the analysis of a single late-time configuration is shown in Fig. 9. The unshocked blue region has a clear distinction to the uniaxially compressed elastic precursor, shown in green. Within the uniaxially compressed region, nucleation of another phase (shown in magenta) is revealed. The transformed magenta material forms needle-like structures along the direction of maximum shear stress (diagonal). This is typical for martensitic-type phase

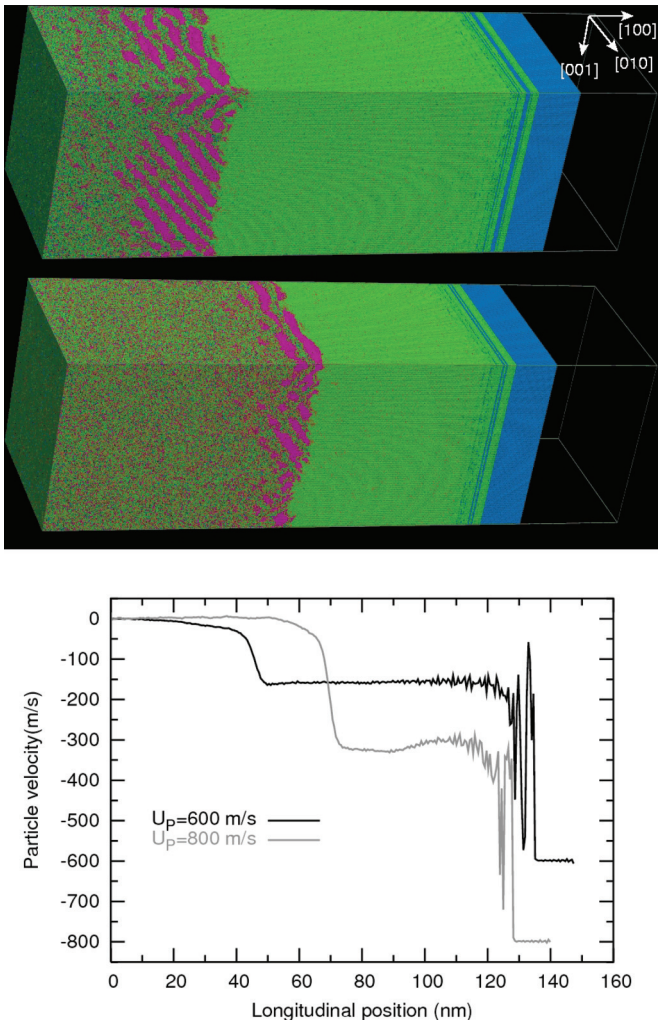

FIG. 7. (Color online) Ga single crystals shocked along the [100] direction shown 35.6 ps after impact with a momentum mirror on the left induced a shock wave traveling to the right. The particle velocity for the top (bottom) sample is $u_p = 600$ m/s (800 m/s). Color coding is as in Fig. 5. An elastic precursor (blue/green) can be seen ahead of the product phase (magenta). For $u_p = 800$ m/s, the material quickly becomes melted or amorphous, as can also be seen for $u_p = 600$ m/s near the piston face. The temperature, pressure, and shock velocity of the elastic (plastic) region for the top and bottom samples are 47.1 K, 11.6 GPa, and 4.4 km/s (317 K, 13.9 GPa, and 2.1 km/s); and 50 K, 12.6 GPa, and 4.4 km/s (471 K, 18.7 GPa, and 2.8 km/s), respectively. Each sample contains 21.5 million atoms in a 47.6 nm × 51.9 nm × 170.5 nm geometry.

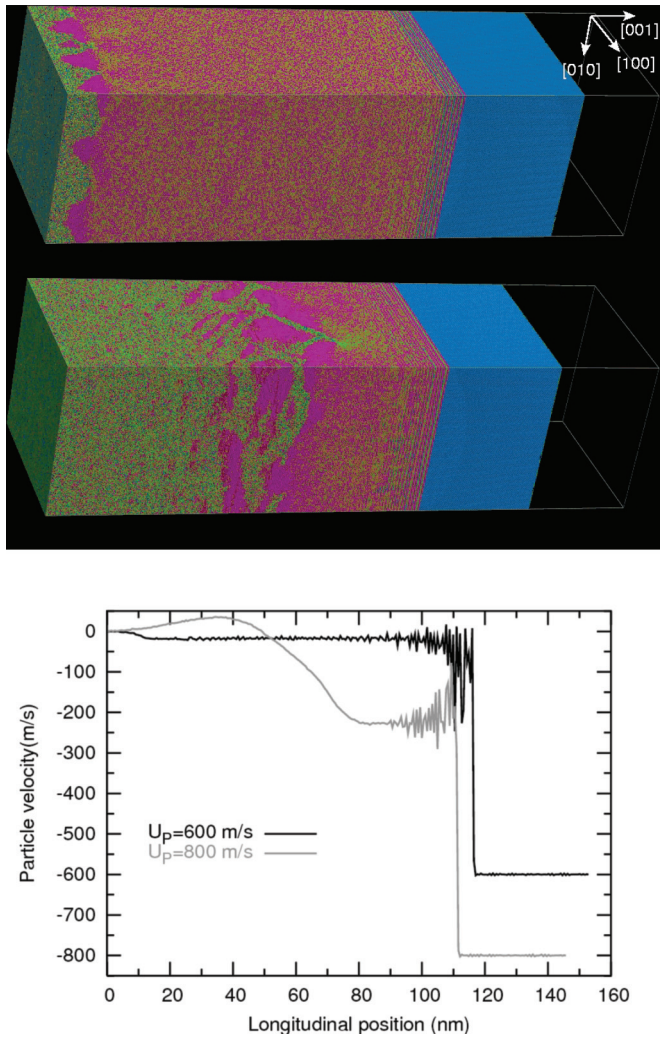

FIG. 8. (Color online) Ga single crystals shocked along the [001] direction shown 35.6 ps after impact with a momentum mirror on the left induced a shock wave traveling to the right. The particle velocity for the top (bottom) sample is $u_p = 600$ m/s (800 m/s). Color coding is as in Fig. 5. An elastic precursor (blue/red) can be seen ahead of the product phase (magenta). For $u_p = 800$ m/s, the material quickly becomes melted or amorphous, as can also be seen for $u_p = 600$ m/s near the piston face. The temperature, pressure, and shock velocity of the elastic (plastic) region for the top and bottom samples are 52 K, 13.5 GPa, and 3.9 km/s (323 K, 13.6 GPa, and 0.85 km/s); and 66 K, 13.5 GPa, and 3.9 km/s (391 K, 17.8 GPa, and 2.7 km/s), respectively. Each sample contains 21.6 million atoms in a 50.6 nm × 47.6 nm × 176.3 nm geometry.

transformations where the enthalpy gain of the new phase is balanced by the surface- and strain-enthalpy. Figure 9(b) shows four different cut-outs from the whole sample, which is shown in Fig. 9(a). Those four cut-outs were taken from two different variants of the transformed region, as well as the uniaxially compressed precursor and the A11 ground state. Figure 9(c) shows a linear intensity plot of the Fourier transformation of the cut-outs excluding the transformed magenta material, which is separately shown in the Fig. 9(d). The peaks of the Fourier transformation density plot correspond to the peaks obtained by x-ray diffraction with a beam in [001] direction as denoted in Fig. 9(a). By measuring the distance between the diffraction peaks, one can nicely see that the distance of peaks in [100] does not change as the sample is not compressed in this direction. However, peaks in the [010] direction are elongated by 1.1, corresponding to a compression in this direction of 9%, which is in line with measured densities in this region. According to the elongated distance of the diffraction peaks of the green elastic material in the mixed phase region, a compression of 5% and 8% in the [010] and [100] directions is observed, respectively. This results in a volume compression of 17%, which is slightly larger than the average volume compression of 13% for this region. It can also be seen that the green elastically compressed material in

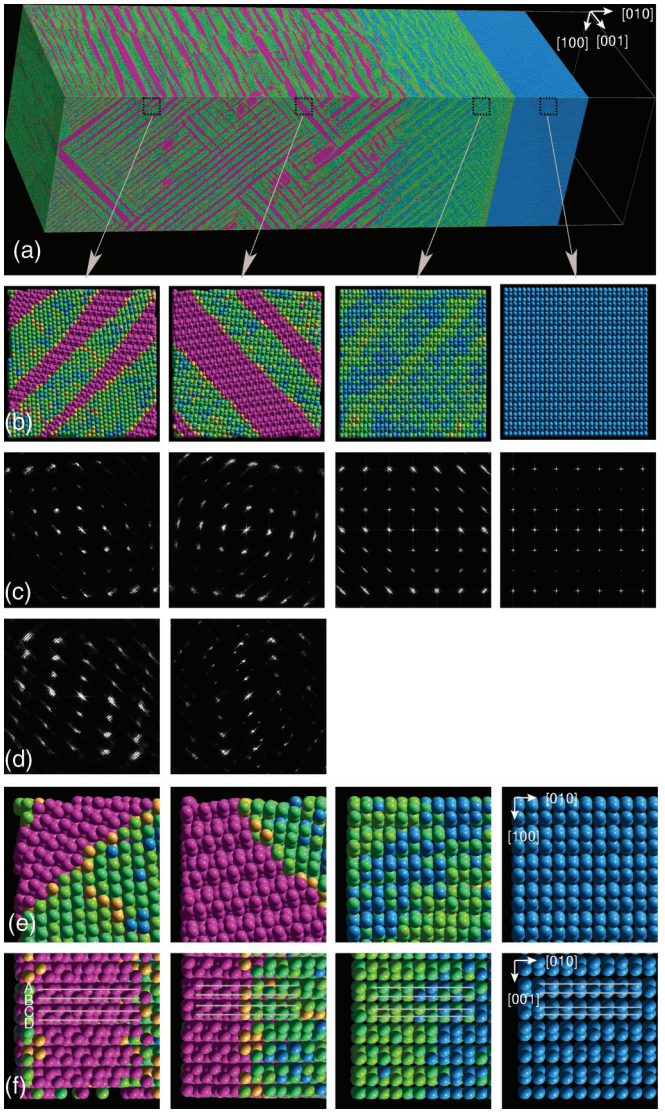

FIG. 9. (Color online) Single-crystal Ga shocked along the [010] direction, 52.9 ps after impact with a momentum mirror on the left induced a shock wave traveling to the right with particle velocity $u_p = 500$ m/s. Color coding is as in Fig. 5. Row (a): the A11 ground state (blue) is uniaxially compressed (green) before needles of the product phase (magenta) are formed. Row (b): close-ups of the regions marked in (a). Row (c): a linear intensity plot of the Fourier transformation of the cut-outs excluding the transformed (magenta) material, shown separately in row (d). Row (e): the upper left corner of the close-ups of row (b), also shown "from above" in row (f). Here, it can be seen that the magenta phase is actually the β phase with a stacking fault. We attribute this stacking fault to the geometry of the phase transformation, i.e., it is easier for the atoms to transform from the A11 structure (which has an ABCD stacking sequence in the [001] direction) into the β-stacking fault structure (which has an ABCD stacking sequence in the [100] direction), as compared to the β phase that has an AB stacking sequence in the [100] direction. The temperature, pressure, and shock velocity of the elastic (plastic) region are 11 K, 8.3 GPa, and 3.9 km/s (46 K, 11.2 GPa, and 3.06 km/s). This sample contains 50.3 million atoms in a 71.1 nm $\times$ 58.2 nm $\times$ 237.5 nm geometry.

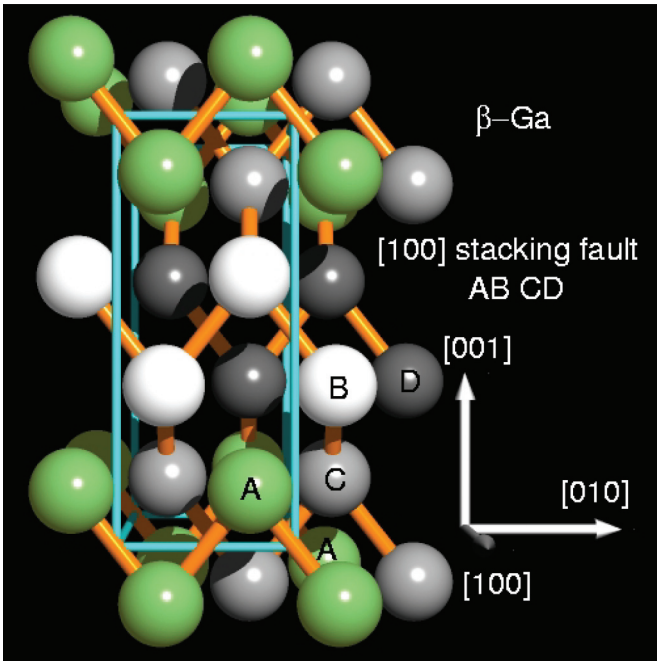

FIG. 10. (Color online) The β-Ga structure with a stacking fault in the [100] direction is observed as a product phase under shock loading in the atomistic simulations presented here.

this region is slightly rotated around the [001]-direction, with the corresponding transformed magenta material rotated in the opposite direction [see Figs. 9(a) and 9(d)]. Furthermore, the two variants are rotated also in the opposite direction.

In order to analyze the transformed magenta phase more closely, a further zoom-in of the top-left corner of the cut-outs shown in Fig. 9(b) is presented in Fig. 9(e). A close visual inspection of the magenta phase reveals an order that resembles that of the β-phase shown in Fig. 3 along [100]. However, the distances of the peaks in Fig. 9(d) reveal a unit cell in this direction that is about twice as large as the β phase. Rotating the tiny regions of Fig. 9(e) around [010] by 90° shows that the stacking sequence of the newly found magenta phase is ABCD and not AB as in the β phase in the [100] direction [see Fig. 9(f)]. Therefore we refer to this newly discovered phase as the β-stacking fault phase (see Fig. 10). The diffraction analysis of stripes are in good agreement with position analysis taken from Figs. 9(e) and 9(f) and are also in good agreement with the symmetry of the β-stacking fault phase symmetry shown in Fig. 10.

Radial distribution functions of the A11 ground state, the uniaxially compressed precursor, and the mixed-phase region of Fig. 9 are shown in Fig. 11. We also indicate the neighbor distance weights of the β-stacking fault phase as symbols. It can be seen that the newly formed peaks in the mixed phase region correspond to the neighbor distances of the β-stacking fault phase, or peaks of the (uniaxially compressed) A11-phase. The radial distribution functions for the mixed-phase product formed during shock compression in the other two directions, [100] (see Fig. 7) and [001] (see Fig. 8), are also similar to that shown in Fig. 11, with the differences attributable to slight variations in the strain state

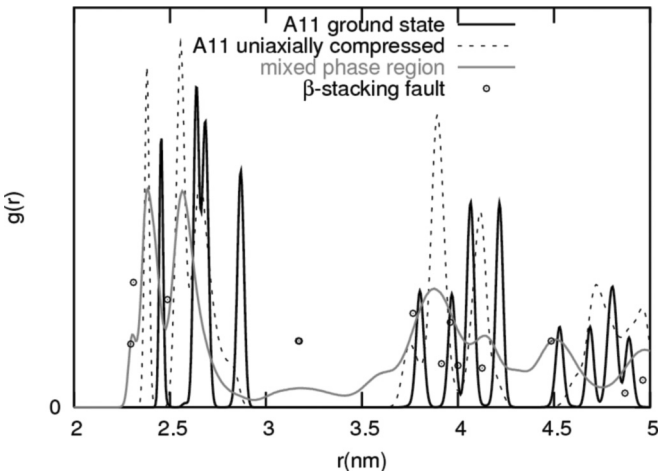

FIG. 11. Radial distribution functions for the A11 ground state, A11 uniaxially compressed in [010] direction, and the mixed phase region for a shock strength of $u_p = 500$ m/s (see Fig. 9). The open circles indicate the number of neighbors (scaled by the squared distance) for the β-stacking fault structure with the lattice parameters obtained from the atomic positions (see Table I).

of the β-stacking fault phase as a result of its formation under different loading conditions.

F. MEAM and first-principles electronic structure calculations of the Ga energy landscape

In order to analyze the energy landscape of various Ga crystal phases as described by the MEAM formalism, "cold curves" plotting energy as a function of volume at $T = 0$ are shown in Fig. 12. For each crystal symmetry, lattice parameters, including dimer distances and orientation (if applicable), are optimized at each volume to provide the minimum energy structure and its energy. In case of the β structure, we found two sets of parameters that were

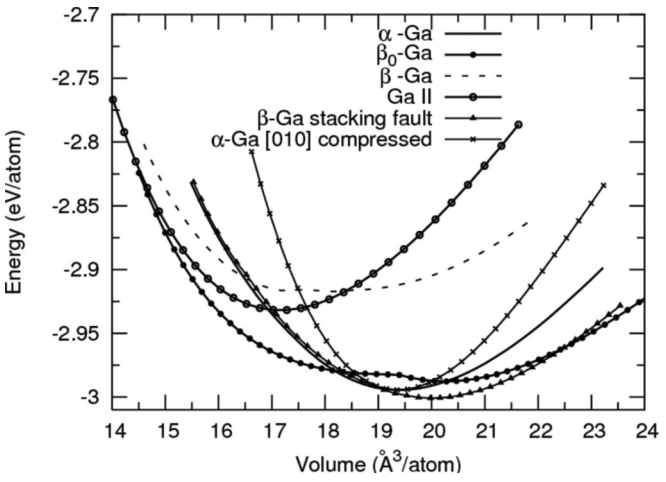

FIG. 12. Energy as a function of volume (cold curves) for various structures as obtained by the MEAM formalism. The β structure is based on the experimentally observed lattice constants and only optimized such that the structure does not overcome the barrier to reach the β_0 phase that has the same symmetry but different sets of lattice parameters and is lower for the applied MEAM formalism.

TABLE I. Lattice constants as obtained by the MEAM potential (values in parenthesis indicate experimental data[34,35] as summarized in Refs. 36 and 21. a, b, and c denote the lattice parameters in the [100], [010], and [001] directions, respectively. The y and z values are internal coordinates. For the A11 structure, the y and z values give the fractions of the projections of the atoms in the dimer onto the orthorhombic unit cell in the [010] and [001] directions, respectively (see Fig. 1). For the β structures, the value of z indicates the absolute lengths of the projections of the atoms onto the unit cell in [001] direction (the projection onto the [010] directions is always 0.25 by symmetry) (see Fig. 3). In case of the β-stacking fault (β-sf) structure, the value of y and a determine the distances between [100] planes: AB distance = CD distance $=(1-y)a/2$, BC distance $=(1+y)a/2$ (see Fig. 10). The asterisk denotes lattice parameters found in the product phase for shock simulations in the [010] direction with $u_p = 500$ m/s (see Fig. 9).

	A11	β	β_0	β-sf	β-sf*
a (Å)	4.526 (4.510)	3.053 (2.766)	4.080	4.060	3.63
b (Å)	4.812 (4.516)	3.137 (3.333)	2.813	2.797	3.17
c (Å)	7.108 (7.645)	7.586 (8.052)	7.067	7.039	5.49
y	0.0670 (0.0785)			0.0435	0.121
z	0.1666 (0.1525)	0.147 (0.131)	0.1667	0.1636	0.153

separated by an energy barrier; the first β structure is related to the experimental parameter set. The second set of lattice parameters (β_0 in Fig. 12) is lower in energy for all volumes considered here, and its cold curve exhibits two minima. Also noteworthy is the fact that using the β-stacking fault phase has the lowest energy of all phases, which we considered, according to this MEAM potential. The lattice parameters at which the energy has a minimum for the different symmetries are summarized in Table I.

In order to determine whether the MEAM formalism is capable of predicting the stability of this newly discovered β-stacking fault structure (see Fig. 12), we performed *ab initio* density functional theory (DFT) calculations employing the Vienna *ab initio* simulation package (VASP).[37] The projector-augmented wave (PAW) method[37,38] was used to treat the ion-electron interaction. All calculations were done using the generalized gradient approximation (GGA) with the Perdew-Wang 91 functional.[39,40] A plane-wave cutoff energy of 300 eV was found to give sufficiently accurate structural energies and converged stresses. The integration over the Brillouin zone was performed using the Monkhorst-Pack (MP) scheme[41] using 2541 and 6975 MP k points.

In Fig. 13, we show the cold curves for the A11 and β-stacking fault structures. The A11 structure has a four-atom orthorhombic unit cell with the $Cmca$-D_{2h}^{18} space group, while the β-sf structure has an eight-atom orthorhombic unit cell with a $Pbcm$-D_{2h}^{11} space group. The unrelaxed curves were obtained by relaxing the cell lengths at constant volume but keeping the relative positions of the atoms in the unit cell to those based on the coordinates obtained at the MEAM ground states. It can be seen that the relation between the two cold curves is similar for both MEAM and VASP, suggesting that MEAM is indeed capable of describing the energetic stability rather well. Although the absolute energies are different, this is expected when performing electronic structure calculations.

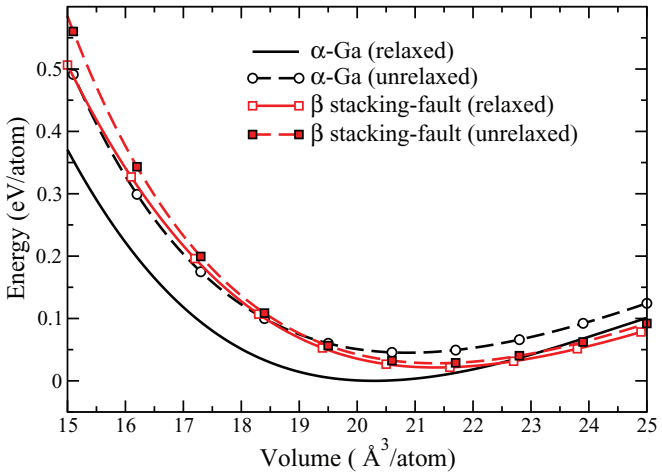

FIG. 13. (Color online) Energy as a function of volume for the A11 and β-stacking fault structure obtained by electronic structure calculations (VASP code) with and without internal relaxation. The unrelaxed curves were obtained by minimizing the cell shape while fixing the relative coordinates of the atomic positions in the unit cell to those values taken from the minimum in energy obtained by the MEAM formalism (Table I). The relaxed curves were obtained by additionally minimizing these initial MEAM atomic coordinates, of the A11 and β-stacking fault unit cells as detailed in the text. The energies shown here are measured with respect to the cohesive energy of the relaxed A11 structure.

Further evidence of the stability of the β-stacking fault structure requires relaxation of the internal degrees of freedom in addition to structural relaxation (c/a ratio at fixed volume). The energy curves of the so-relaxed A11 and β-stacking fault Ga structures are also shown in Fig. 13. The internal degrees of freedom of the A11 structure were fully relaxed, while those of the β-sf structure were relaxed only in the a-b direction (X-Y plane) of the unit cell while the positions along the c axis were fixed in order to prevent structural changes during the energy minimization. Upon relaxation, the experimentally observed A11 ground state does indeed have the lowest energy, but the β-stacking fault structure has a metastable minimum which may be favored under tension. It should be noted that the constrained relaxation of the β-sf structure's internal degrees of freedom results in a relatively small change in the relaxed energy/atom of this structure with respect to the unrelaxed one.

To investigate the mechanical stability of the β-sf structure, we calculated via DFT lattice dynamics, the harmonic phonon bands at zero pressure and temperature. The phonon calculations were carried out employing supercells with 96 and 128 atoms. The phonon dispersions of the β-sf structure reveal imaginary frequencies along the Γ-Z and Γ-R of the $Pbcm$ Brillouin zone indicative of a negative C_{44} elastic constant. This is more likely due to the imposed symmetry constraint during the relaxation of the internal degrees of freedom and suggests that the interfacial energy and local strain at the phase boundaries play a role in stabilizing this new phase. Furthermore, the transition does not seem to be kinetically driven as only a small fraction of this phase appears within the uniaxially compressed α phase. This suggests that this new type of stacking fault is closely tied to the geometry of the phase transformation, i.e., it is easier for the atoms to transform from the α (A11) structure (which has an ABCD stacking sequence in the [001] direction) into the β-sf structure (which has an ABCD stacking sequence in the [100] direction), as compared to the β phase, which has an AB stacking sequence in the [100] direction. First-principles calculation of the actual A11-β-sf sequence observed in the MD simulations would require hundreds of atoms.

The cold-curve calculations—using both MEAM and electronic structure methods—were only performed to see whether the β-stacking fault phase is energetically favorable. *Ab initio* phonon band calculations suggest that this new phase is unstable at 0 K. This is most likely due to the imposed symmetry constraint during minimization. Temperature effects and strain energies might play an important role in the stability of this new stacking fault structure. However, in order to make conclusive statements about the possible phase stability of the β-stacking fault structure, a more complete relaxation of the unit cells used in the electronic structure calculations would be necessary, as would a self-consistent temperature dependent analysis of the phonon spectra.[42] However, these would require significantly more effort and are beyond the scope of the current work.

Finally, we note that De Koning *et al.* recently found by employing the same MEAM and using first-principles calculation a new phase under heating for elemental Ga[43] different from the one found here under shock loading. This demonstrates the complexity of Ga and the variety of metastable phases of this elemental solid.

IV. CONCLUSION AND OUTLOOK

Our NEMD calculations presented here suggest the existence of a new phase for Ga. Because of the similarity to the β structure and the stacking fault nature of this phase, it is termed as β-stacking fault structure. It would be interesting to see whether experimental efforts could confirm the newly predicted shock-induced β-stacking fault structure, similar to studies performed on the shock-induced phase transformations in iron.[13,14] Since the β-stacking fault structure has been found to be energetically competitive—both by the classical MEAM potential and electronic structure calculations—this might be another metastable phase that can occur during nonequilibrium conditions. Furthermore, theoretical and experimental investigation on polycrystalline Ga—similar to studies performed for iron[44]—would shed further light on the fascinating topic of shock-induced phase transformations in polymorphic materials.

ACKNOWLEDGMENTS

We would like to thank Brad Lee Holian (Los Alamos) for many interesting discussions. This work was carried out under the auspices of the National Nuclear Security Administration of the U.S. Department of Energy at Los Alamos National Laboratory under contract No. DE-AC52-06NA25396, with funding by the Advanced Simulation and Computing (ASC) program.

*kadaukai@yahoo.com
†cherne@lanl.gov
‡rravelo@utep.edu
§tcg@lanl.gov

[1]R. R. Moskalyk, Miner. Eng. **16**, 921 (2003).
[2]S. S. Hecker, Los Alamos Sci. **26**, 290 (2000).
[3]M. I. McMahon and R. J. Nelmes, Chem. Soc. Rev. **35**, 943 (2006).
[4]O. Degtyareva, M. I. McMahon, D. R. Allan, and R. J. Nelmes, Phys. Rev. Lett. **93**, 205502 (2004).
[5]G. E. Duvall and R. A. Graham, Rev. Mod. Phys. **49**, 523 (1977).
[6]B. L. Holian and P. S. Lomdahl, Science **280**, 2085 (1998).
[7]T. C. Germann, B. L. Holian, P. S. Lomdahl, and R. Ravelo, Phys. Rev. Lett. **84**, 5351 (2000).
[8]O. Kum, J. Appl. Phys. **93**, 3239 (2003).
[9]E. M. Bringa, J. U. Cazamias, P. Erhart, J. Stölken, N. Tanushev, B. D. Wirth, R. E. Rudd, and M. J. Caturla, J. Appl. Phys. **96**, 3793 (2004).
[10]M. M. Budzevich, V. V. Zhakhovsky, C. T. White, and I. I. Oleynik, Phys. Rev. Lett. **109**, 125505 (2012).
[11]K. Kadau, T. C. Germann, P. S. Lomdahl, and B. L. Holian, Science **296**, 1681 (2002).
[12]K. Kadau, T. C. Germann, P. S. Lomdahl, and B. L. Holian, Phys. Rev. B **72**, 064120 (2005).
[13]D. H. Kalantar, J. F. Belak, G. W. Collins, J. D. Colvin, H. M. Davies, J. H. Eggert, T. C. Germann, J. Hawreliak, B. L. Holian, K. Kadau *et al*., Phys. Rev. Lett. **95**, 075502 (2005).
[14]J. Hawreliak, J. D. Colvin, J. H. Eggert, D. H. Kalantar, H. E. Lorenzana, J. S. Stölken, H. M. Davies, T. C. Germann, B. L. Holian, K. Kadau *et al*., Phys. Rev. B **74**, 184107 (2006).
[15]R. E. Rudd, T. C. Germann, B. A. Remington, and J. S. Wark, MRS Bulletin **35**, 999 (2010).
[16]E. Jaramillo, T. D. Sewell, and A. Strachan, Phys. Rev. B **76**, 064112 (2007).
[17]M. J. Cawkwell, K. J. Ramos, D. E. Hooks, and T. D. Sewell, J. Appl. Phys. **107**, 063512 (2010).
[18]N. Gunkelmann, E. M. Bringa, K. Kang, G. J. Ackland, C. J. Ruestes, and H. M. Urbassek, Phys. Rev. B **86**, 144111 (2012).
[19]M. I. Baskes, Phys. Rev. B **46**, 2727 (1992).
[20]M. I. Baskes, Mater. Chem. Phys. **50**, 152 (1997).
[21]M. I. Baskes, S. P. Chen, and F. J. Cherne, Phys. Rev. B **66**, 104107 (2002).
[22]J. P. Biersack and J. F. Ziegler, Nucl. Instrum. Methods Phys. Res. **194**, 93 (1982).
[23]P. S. Lomdahl, P. Tamayo, N. G. Jensen, and D. M. Beazley, in *Proceedings of Supercomputing '93*, edited by G. S. Ansell (IEEE Computer Society Press, Los Alamitos, CA, 1993), p. 520.
[24]D. M. Beazley and P. S. Lomdahl, Comput. Phys. **11**, 230 (1997).
[25]K. Kadau, T. C. Germann, and P. S. Lomdahl, Int. J. Mod. Phys. C **17**, 1755 (2006).
[26]T. C. Germann and K. Kadau, Int. J. Mod. Phys. C **19**, 1315 (2008).
[27]K. Kadau, T. C. Germann, and P. S. Lomdahl, Int. J. Mod. Phys. C **15**, 193 (2004).
[28]J. N. Fritz and W. J. Carter, Los Alamos National Laboratory Tech. Rep. LA-13844-MS, 2001 (unpublished).
[29]F. J. Cherne, M. I. Baskes, T. C. Germann, R. J. Ravelo, and K. Kadau, AIP Conf. Proc. **706**, 281 (2004).
[30]M. S. Daw and M. I. Baskes, Phys. Rev. B **29**, 6443 (1984).
[31]R. Harrison, A. F. Voter, and S.-P. Chen, in *Atomistic Simulation of Materials*, edited by V. Vitek and D. J. Srolovitz (Plenum Press, New York, 1989), pp. 219–221.
[32]See Supplemental Material at http://link.aps.org/supplemental/10.1103/PhysRevB.88.144108 for a movie of shocked gallium with number of neighbor coloring of atoms. Shock wave with particle velocity $u_p = 500$ m/s traveling along the [010] direction in a Ga single crystal containing about 50 million atoms, from which the snapshot analyzed in Fig. 9 is taken. The simulation movie covers about 74 ps (73 000 time steps) and colors atoms as shown in Fig. 9.
[33]See Supplemental Material at http://link.aps.org/supplemental/10.1103/PhysRevB.88.144108 for a movie of shocked gallium with potential energy coloring of atoms. Same simulation as Ref. 32, but coloring of the atoms are according their potential energy from −3.053 to −2.700 eV.
[34]R. Wyckoff, *Crystal Structures* (Wiley, New York, 1962).
[35]L. Bosio, A. Defrain, H. Curien, and A. Rimsky, Acta Christalogr. B **25**, 995 (1969).
[36]M. Bernasconi, G. L. Chiarotti, and E. Tosatti, Phys. Rev. B **52**, 9988 (1995).
[37]G. Kresse and J. Furthmuller, Phys. Rev. B **54**, 11169 (1996).
[38]P. E. Blochl, Phys. Rev. B **50**, 17953 (1994).
[39]J. P. Perdew, in *Electronic Structure of Solids '91*, edited by P. Ziesche and H. Eschrig (Akademie-Verlag, Berlin, 1991), Vol. 91, p. 11.
[40]J. P. Perdew, J. A. Chevary, S. H. Vosko, K. A. Jackson, M. R. Pederson, D. J. Singh, and C. Fiolhais, Phys. Rev. B **46**, 6671 (1992).
[41]H. J. Monkhorst and J. D. Pack, Phys. Rev. B **13**, 5188 (1976).
[42]P. Souvatzis, O. Eriksson, M. I. Katsnelson, and S. P. Rudin, Phys. Rev. Lett. **100**, 095901 (2008).
[43]M. de Koning, A. Antonelli, and Diego Alejandro Carvajal Jara, Phys. Rev. B **80**, 045209 (2009).
[44]K. Kadau, T. C. Germann, P. S. Lomdahl, R. C. Albers, J. S. Wark, A. Higginbotham, and B. L. Holian, Phys. Rev. Lett. **98**, 135701 (2007).